Excimer of 9-Aminoacridine Hydrochloride Hydrate in Confined Medium: An Integrated Experimental and Theoretical Study

ARTICLE *in* THE JOURNAL OF PHYSICAL CHEMISTRY A · JANUARY 2013

Impact Factor: 2.69 · DOI: 10.1021/jp3103639 · Source: PubMed

4 AUTHORS, INCLUDING:

Brotati Chakraborty
Bejoy Narayan Mahavidyalaya, Itachuna, Hoo…
12 PUBLICATIONS **126** CITATIONS
SEE PROFILE

Dhananjay Bhattacharyya
Saha Institute of Nuclear Physics
116 PUBLICATIONS **1,105** CITATIONS
SEE PROFILE

THE JOURNAL OF PHYSICAL CHEMISTRY A

Article

pubs.acs.org/JPCA

Excimer of 9-Aminoacridine Hydrochloride Hydrate in Confined Medium: An Integrated Experimental and Theoretical Study

Piyali Mitra,[†,∥] Brotati Chakraborty,[§,∥] Dhananjay Bhattacharyya,[‡] and Samita Basu*[,†]

[†]Chemical Sciences Division and [‡]Computational Science Division, Saha Institute of Nuclear Physics, 1/AF, Bidhannagar, Kolkata 700064, India

[§]Department of Chemistry, Adamas Institute of Technology, Barasat-Barrackpore Road, Barbaria, P.O. Jagannathpur, North 24 Parganas, Pin -700126, India

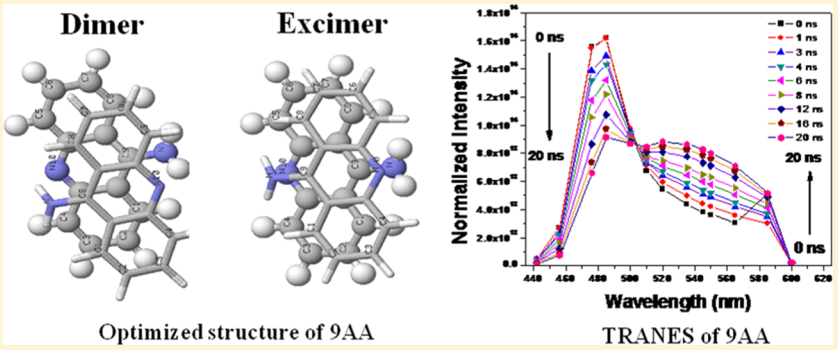

ABSTRACT: We aim to find out the extent of stability of the excimer of 9-aminoacridine hydrochloride hydrate (9AA), a prospective PDT drug, in different confined media with varying cavity size. When confined in cetyltrimethyl ammonium bromide micelles, although at low concentration of 9AA, only a single distinct peak (λ_{max} at 460 nm) with a shoulder at 485 nm is observed in steady-state fluorescence spectrum, yet with increase in concentration the peak and the shoulder merge with simultaneous emergence of another peak at 535 nm, which is assigned to excimer. Similar behavior is also observed in Triton-X, crown ether, α-cyclodextrin, β-cyclodextrin, and homogeneous aqueous medium. The formation of excimer, which reflects the extent of confinement of 9AA, is maximum in β-cyclodextrin followed by others. Steady-state and time-resolved fluorescence studies along with TRES and TRANES analyses coupled with anisotropy data and transient absorption studies reveal the presence of monomer−dimer equilibrium of 9AA in the excited state. Molecular modeling indicates that the structure of excimer is stabilized by locking of the two monomeric species via four hydrogen bonds formed between the amino-H and imino-N of 9AA monomers, whereas the dimer in the ground state has only two such hydrogen bonds.

1. INTRODUCTION

The phenomenon of dimerization or aggregation of organic dyes is highly significant in the fields of biology, textile, colloids, photography, and so on.[1] A variety of experimental methods, viz., absorption,[2] fluorescence,[3] NMR,[4,6] FTIR,[5] and mass spectroscopies,[6] as well as high-end theoretical techniques[7−12] have been utilized to study monomer−dimer equilibrium. Spectroscopic investigation of aggregation in the excited state has received immense attention.[13,14]In fact, the study of aggregation of organic dyes has drawn the interest of researchers from a variety of domains.[15] Moreover, the use of organized media to modulate the rate of aggregation resulting in modulation of monomer−dimer equilibrium has been reported by a number of scientists.[15a,16]

Acridine and its derivatives are well known for their pharmacological and biological significance. In the recent past, our group has been engaged in exploring the photochemical interactions of acridine and some of its important derivatives with organic amines, nucleobases, and their nucleosides, serum albumins, cucurbiturils, and so on.[17−27] Recently, we have started working with another well known derivative of acridine, that is, 9-aminoacridine hydrochloride hydrate (9AA) (depicted in Figure 1), which has been found to be a DNA intercalator as well as an antibacterial and anticancer drug.[28−33] An additional interesting feature about 9AA is that it belongs to those rare classes of compounds, which readily form dimers at higher concentration.[34−38] It has been found that the formation of 9AA dimer is greatly favored when the drug is in the amino form.[36−38]The study of the aggregation phenomen-

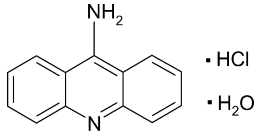

Figure 1. Structure of 9AA.

Received: October 19, 2012
Revised: January 24, 2013
Published: January 24, 2013

on of 9AA is of significance because of the fact that similar to many other acridine derivatives 9AA is a prospective drug in photodynamic therapy (PDT)[39] and the state of aggregation of a dye determines its photophysical and binding properties, which in turn may affect the efficiency of PDT.[40] The influence of state of aggregation on singlet oxygen production quantum yield, which is an essential feature of PDT sensitizer, has been reported using a large number of porphyrin derivatives.[41−43] We aim to delve deeper into the study of monomer−dimer equilibrium of 9AA in homogeneous as well as in a number of heterogeneous media using spectroscopic tools like absorption and fluorescence spectroscopies and also laser flash photolysis technique. Theoretical studies have also been performed to corroborate the experimental findings. Although literature shows that 9AA dimerizes at higher concentration in aqueous homogeneous medium, yet we have attempted to find out the lifetime of the dimer in different heterogeneous confined medium with varying cavity size. We have also tried to optimize the structure of dimer of 9AA using molecular modeling, from which its dimension as well as relative energy and stability in ground and excited states could be obtained. Exploration of the monomer−dimer equilibrium in various confined media is carried out with the objective to mimic biological systems, keeping in mind the use of 9AA as a sensitizer in PDT.

2. EXPERIMENTAL METHODS

2.1. Materials. 9AA, α-cyclodextrin (CD), β-CD and crown ether (18-*crown*-6) were purchased from Sigma. Cetyltrimethyl ammonium bromide (CTAB) and Triton-X were procured from Aldrich and Merck, respectively. Water was triply distilled before use.

2.2. Apparatus. The absorption spectra were recorded on a Jasco V-650 absorption spectrophotometer at 298 K within a wavelength range of 300 to 550 nm using a pair of 1 × 1 cm path length quartz cuvettes. Steady-state fluorescence excitation spectra were recorded in a Spex Fluoromax-3 spectrofluorimeter using 1 × 1 cm path length quartz cuvettes at 298 K. The fluorescence spectra were recorded from 410 to 750 nm, keeping excitation wavelength (λ_{ex}) at 400 nm. Steady-state anisotropy measurements were carried out in a Hitachi-700 spectrophotometer. The anisotropy values were determined using the following equations[44]

$$r = \frac{(I_{VV} - G{\cdot}I_{VH})}{(I_{VV} + 2G{\cdot}I_{VH})} \quad (1)$$

G factor is determined by

$$G = \frac{I_{HV}}{I_{HH}} \quad (2)$$

In the above two equations, r is the steady-state anisotropy and I_{VV} and I_{VH} are the emission intensities when excitation polarizer is vertically oriented and the emission polarizer is oriented vertically and horizontally, respectively. I_{HV} and I_{HH} are the emission intensities when the excitation polarizer is oriented horizontally and the emission polarizer is oriented vertically and horizontally, respectively. Fluorescence lifetime in singlet state was measured using a diode laser-based JobinYvon Horiba picosecond-resolved time-correlated-single-photon-counting (TCSPC) spectrometer with excitation wavelength at 375 nm. The pulsing frequency of diode laser is 1 MHz. The full width at half-maximum (fwhm) of the instrument response function (IRF) is 250 ps, and the resolution is 28 ps per channel. The data were fitted to multiexponential functions after deconvolution of the IRF by an iterative reconvolution technique using IBH DAS 6.2 data analysis software. Analysis of the fluorescence decay data $I(t)$ was done using the following equation

$$I(t) = \sum_i B_i \exp\left(\frac{-t}{\tau_i}\right) \quad (3)$$

where B_i and τ_i are the pre-exponential factor and the fluorescence lifetime, respectively. The values of reduced χ^2 and residuals serve as the parameters for goodness of the fit. Using the steady-state and time-resolved fluorescence data the time-resolved emission spectra (TRES) and time-resolved-area-normalized-emission spectra (TRANES) were constructed. TRES was constructed by measuring the fluorescence decays across the emission spectrum (442−600 nm) at particular intervals. The fitted fluorescence decays were scaled with the steady -state fluorescence intensities.[45,46]The fractional contribution of each component of the fluorescence spectrum at the wavelength measurement was calculated according to the following equation

$$I_i(\lambda) = \frac{a_i\tau_i}{\sum a_i\tau_i} \quad (4)$$

where, $I_i(\lambda)$ is the fractional contribution and a_i and τ_i are the relative amplitude and lifetime of the ith component, respectively. Now the reconstruction of the time-resolved spectra at different time t was performed using the best fitting parameters as suggested by Maroncelli and Fleming.[47] A nanosecond flash photolysis setup (Applied Photophysics) containing a Nd:YAG (Lab series, Model Lab150, Spectra Physics) laser was used for the measurement of transient absorption spectra. The sample was excited at 355 nm (fwhm = 8 ns) laser light. Transients were monitored through absorption of light from a pulsed xenon lamp (150 W). The photomultiplier (R298) output was fed into an Agilent Infiniium oscilloscope (DSO8064A, 600 MHz, 4Gs/s), and the data were transformed to a computer using the IYONIX software. The software origin 8 was used for curve fitting. The solid curves were obtained by connecting the points using B-Spline option. The samples were deaerated by passing pure argon gas for 20 min prior to each experiment. No degradation of the samples was observed during the experiments.

2.3. Modeling and Computational Methods. Extensive model building followed by structural optimization and energy calculation using dispersion-corrected density functional theory (DFT-D) were carried out to delineate the structures and also to measure the interaction energies of monomer and dimer both in ground and excited states. The molecular structure of 9AA was constructed with the help of MOLDEN software,[48] and the dimer of 9AA was created using Discovery studio.[49] The ground and excited states of monomer and dimer of 9AA were optimized by the standard wB97XD/631G (2d, 2p),[50]which is a dispersion-corrected density functional theory (DFT)-based approach using Gaussian 09.[51]Time-dependent DFT (TD-DFT)[52−58]method was used for optimization of structure of excimer using same basis set and DFT functional. Interaction energy between the monomer units of the dimer and excimer was calculated considering basis set superposition error (BSSE) and deformation correction using the following equation.

dx.doi.org/10.1021/jp3103639 | J. Phys. Chem. A 2013, 117, 1428−1438

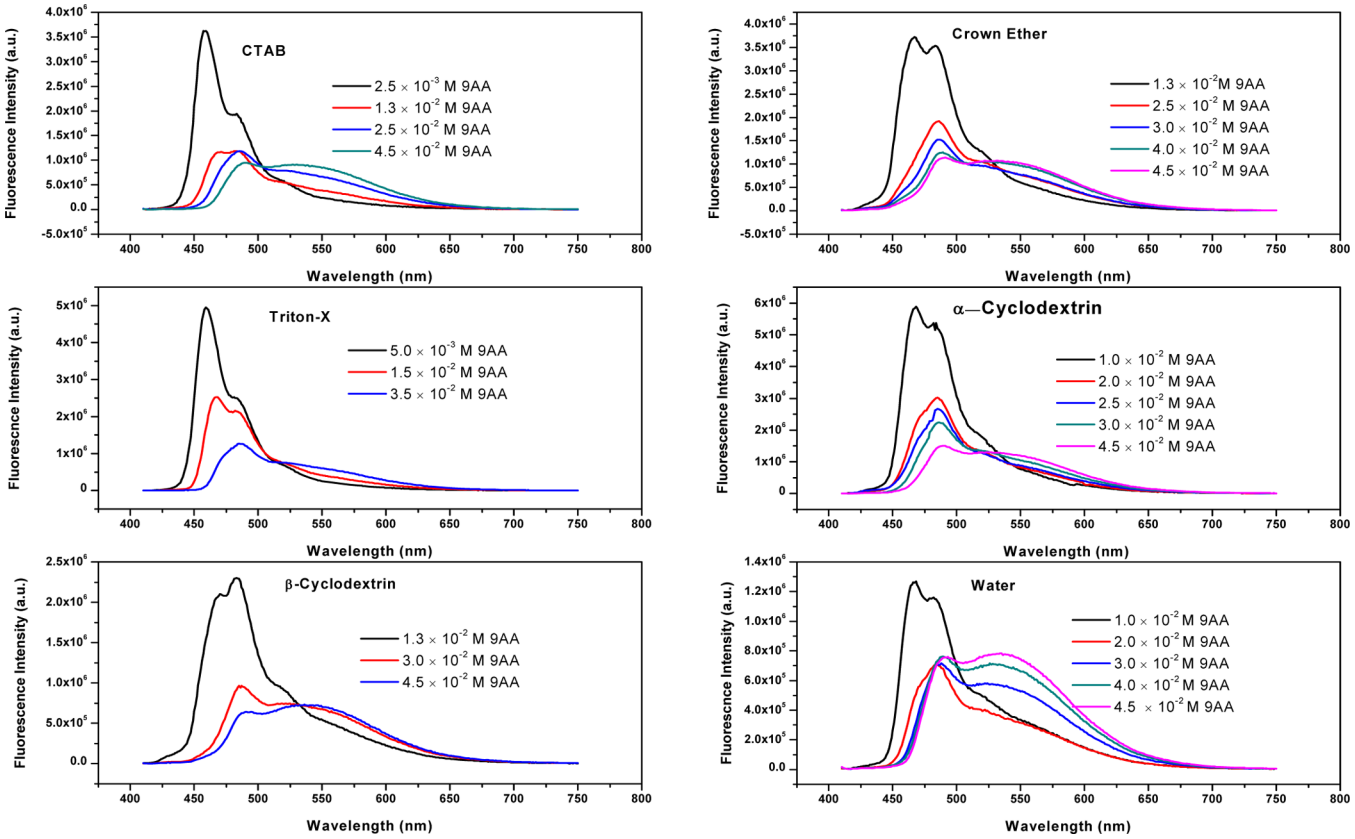

Figure 2. Fluorescence spectra of 9AA with variation in concentration in CTAB, crown ether, Triton-X, α-cyclodextrin, β-cylcodextrin, and water (λ_{ex} = 400 nm).

Table 1. Lifetime of Monomer at High and Low Concentration of 9AA in Various Media (λ_{ex} = 375 nm)

medium	λ_{em} (nm)	[9AA] (M)	B1	B2	B3	τ_1 (ns)[a]	τ_2 (ns)[a]	τ_3 (ns)[a]	χ^2
water	485	5.0×10^{-5}	100.00			15.70			1.16
		3.0×10^{-2}	67.30	32.70		3.66	20.83		1.53
CTAB	485	5.0×10^{-5}	98.94	1.06		15.31	7.73		1.01
		2.5×10^{-2}	69.85	4.47	25.69	4.25	0.49	16.66	1.00
β-CD	485	5.0×10^{-5}	98.95	1.05		16.04	7.76		1.05
		3.0×10^{-2}	67.56	5.40	27.04	4.28	0.023	21.90	1.07
α-CD	485	5.0×10^{-5}	96.46	3.54		16.45	8.49		1.25
		2.0×10^{-2}	81.89	4.18	13.93	6.22	0.58	19.26	1.40
Triton-X	485	5.0×10^{-5}	69.60	30.40		10.86	2.78		1.40
		1.5×10^{-2}	71.51	17.32	11.17	5.18	1.38	16.43	1.33
crown ether	485	5.0×10^{-5}	80.41	19.59		15.65	4.95		1.15
		3.0×10^{-2}	69.45	3.67	26.87	4.46	1.45	19.50	1.01

[a] ±5%.

$$E_{int} = E(\text{dimer}) - 2 \times E_{Xo}(\text{monomer}) + \text{BSSE} \quad (5)$$

where E (dimer) and E_{Xo}(monomer) are energies of the optimized structures of 9AA dimer and monomer, respectively.

The BSSE components were calculated by Boys−Bernardi counterpoise method.[59]

3. RESULTS AND DISCUSSION

3.1. Steady-State Fluorescence Studies. The steady-state fluorescence spectrum of 9AA at low concentration (2.5×10^{-3} M) shows a single distinct peak (λ_{max} at 460 nm) with a shoulder at 485 nm in 0.1 M CTAB medium, as depicted in Figure 2. With increase in concentration of 9AA, the peak and the shoulder merge, forming a broad peak centered around 485 nm, accompanied by a decrease in fluorescence intensity with simultaneous emergence of another peak at 535 nm. The species formed at 535 nm is not due to further protonated form of 9AA.[35] The onset of appearance of the new peak begins from around 1.3×10^{-2} M 9AA. The fluorescence intensity at 535 nm increases with increase in concentration of the acridine dye. The steady-state fluorescence spectrum of 9AA shows similar behavior in other confined media like crown ether, α-CD, β-CD, and Triton-X as well as in homogeneous medium water (Figure 2); however, with the variation in medium there is a slight shift in the position of the new peak at red end. It is noteworthy that for low concentration of 9AA (2.5×10^{-3} M in CTAB medium), the positions of the peak around 460 nm, and its shoulder (~485 nm) remain unaltered on variation of

dx.doi.org/10.1021/jp3103639 | J. Phys. Chem. A 2013, 117, 1428−1438

Table 2. Lifetime of Excimer at High and Low Concentration of 9AA in Various Media (λ_{ex} = 375 nm)

medium	λ_{em} (nm)	[9AA] (M)	B1	B2	B3	τ_1 (ns)[a]	τ_2 (ns)[a]	τ_3 (ns)[a]	χ^2
water	545	5.0×10^{-5}	100.0			15.95			1.11
		3.0×10^{-2}	91.84	8.16		22.64	3.28		1.18
CTAB	535	5.0×10^{-5}	96.00	4.00		14.82	3.17		1.30
		2.5×10^{-2}	86.69	11.98	1.33	20.20	4.90	0.39	1.05
β-CD	565	5.0×10^{-5}	99.99	0.01		16.07	7.45		1.12
		3.0×10^{-2}	87.64	10.04	2.31	24.41	11.44	3.36	1.07
α-CD	550	5.0×10^{-5}	99.80	0.20		16.37	8.36		1.09
		3.0×10^{-2}	85.00	13.33	1.68	23.27	5.46	0.24	1.13
Triton-X	545	5.0×10^{-5}	67.01	32.99		10.80	2.84		1.37
		1.5×10^{-2}	63.24	28.74	8.02	20.71	5.94	1.40	1.06
crown ether	545	5.0×10^{-5}	97.78	2.22		16.11	5.98		1.05
		3.0×10^{-2}	88.28	9.83	1.88	22.50	7.48	1.17	1.10

[a] ±5%.

medium, as depicted in Figure 2. The appearance of the new peak at longer wavelength with increase in concentration is an indication of formation of aggregates of 9AA in either ground or excited state. Literature survey suggests that 9AA dimerizes at higher concentration.[34−38,60] However, we have not observed any distinct spectral signature of aggregation on increasing the concentration of 9AA during UV−vis absorption study, thus ruling out the possibility of dimer formation in the ground state. Hence, the lower wavelength fluorescence peak (460−485 nm) of 9AA can be assigned to the monomer, whereas the red-end peak that emerges at high concentration (1.3×10^{-2} M in CTAB medium) can be considered to be the signature of the "excimer", that is, dimer formed in excited state. Therefore, it is to be highlighted that dimerization of 9AA takes place solely in the excited state and not in the ground state.

3.2. Time-Resolved Fluorescence Studies. Fluorescence lifetime of monomer (at 485 nm) and excimer of 9AA at high and low concentrations in various media has been tabulated in Tables 1 and 2.

In aqueous medium, the decay curves of 9AA in low concentration at both 485 and 545 nm fit to a single exponential function (as shown in Tables 1 and 2), indicating the existence of a single species. Moreover, the lifetimes of the transients at both the wavelengths are quite similar (15.70 and 15.95 ns at 485 and 545 nm, respectively), indicating the sole existence of the monomer at low concentration of 9AA. The decay curve at 485 nm (Table 1) for higher concentration of 9AA in aqueous medium fits to biexponential function, implying the presence of two species, with ∼32% contribution from a longer lifetime (20.83 ns) component. The emergence of the longer lifetime component may be assigned to the excimer species. This is accompanied by a shorter component (3.66 ns) with reduced amplitude corresponding to the quenching of the lifetime of the monomer. This means at higher concentration the contribution of monomer is decreased whereas that of the excimer is enhanced. At 545 nm, the decay curve for higher concentration of 9AA in aqueous medium also fits to the biexponential function (Table 2). However, in this case, ∼92% contribution comes from the longer lifetime, which is quite obvious as we have previously assigned the red-end peak around 545 nm to the excimer species of 9AA. In this case, the longer component with higher contribution, that is, 22.64 ns, corresponds to the enhanced lifetime of the excimer, whereas the shorter component with lower contribution, that is, 3.28 ns, corresponds to the lifetime of the monomer. So the species formed at 545 nm is not due to the further protonated form of 9AA as the lifetime of the further protonated form is 29 ns.[35] Thus, the longer lifetime is associated with the excimer, and it is to be noted that the values of the longer components obtained at 485 (20.83 ns) and 545 nm (22.64 ns) are comparable for higher concentration (3.0×10^{-2} M) of 9AA in aqueous medium.

The observation is somewhat different in heterogeneous media, viz. CTAB, α-CD, β-CD, Triton-X, and crown ether. For lower concentration of 9AA, at both 485 nm and corresponding red-end region, the decay curves fit to biexponential function with the major contribution (e.g., 15.31 ns (98.94%) in CTAB medium in Table 1) from the lifetime that is comparable to the lifetime of the monomer obtained in the aqueous medium (as shown in Tables 1 and 2). The shorter lifetime (e.g., 7.73 ns (1.06%) in CTAB medium in Table 1), which has a very small contribution in all of the above confined media, may be attributed to 9AA residing in hydrophobic nonpolar region of the heterogeneous media. However, as 9AA is not soluble in purely nonpolar solvents, it is not possible to report its lifetime in purely hydrophobic nonpolar medium. It is to be noted that the longer lifetime components at low concentration obtained for a particular restricted medium at both 485 nm (Table 1) and corresponding red-end region (Table 2) are comparable, thus confirming their association with the monomer species. At 485 nm, the decay curve for higher concentration of 9AA fits to triexponential function, with a considerable contribution from a longer lifetime component, which possibly corresponds to the excimer species, accompanied by quenching of the lifetime and lowering of relative amplitude of the component attributed to monomer species (Table 1). Similarly, at the red-end region (Table 2), the decay curve for higher concentration of 9AA fits to triexponential function with the major contribution from the longer lifetime, which may be attributed to the excimer species. For example, in the case of crown ether at higher concentration at 545 nm, the lifetime of the excimer is 22.50 ns with ∼88% contribution, whereas the lifetime of the monomer is 7.48 ns with ∼9.80% contribution. The rest is the component with a lifetime of 1.17 ns corresponding to 9AA associated with hydrophobic region of the confined medium.

From the lifetime measurements, it is evident that the excimer has longer lifetime in β-CD and its lifetime in crown-ether is comparable to that of aqueous medium, which in turn is lower than that in β-CD. It is to be mentioned here that the dimension of the excimer is found to be 7 Å × 5 Å. Study of literature shows that the internal radius of the cavity of β-CD

dx.doi.org/10.1021/jp3103639 | J. Phys. Chem. A 2013, 117, 1428−1438

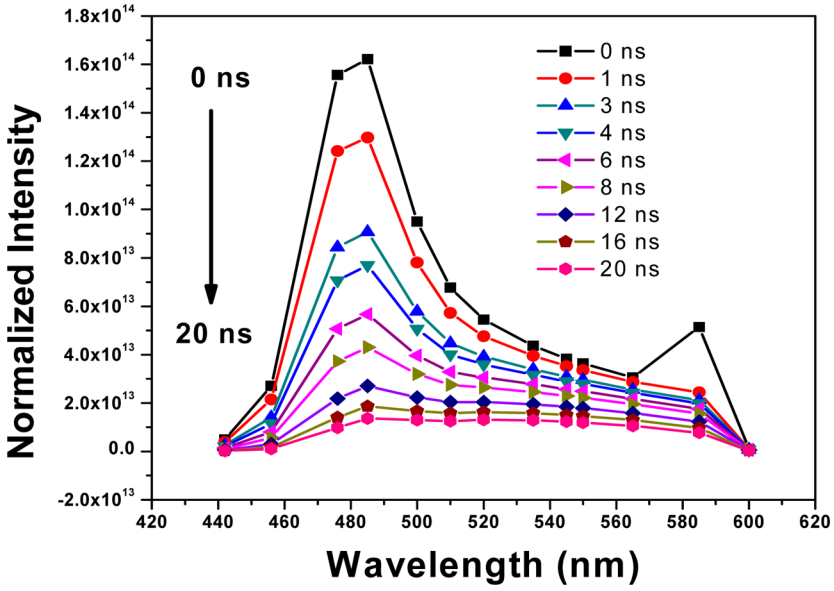

Figure 3. Peak-normalized TRES of 9AA (2.5×10^{-2} M) in 0.1 M CTAB between time 0 and 20 ns.

(7.8 Å)[61]is larger than that of crown ether (2.6 to 3.2 Å).[62] Thus, the inclusion of the excimer within β-CD is possible via axial as well as equatorial encapsulation. However, the dimension of the excimer is such that it can neither equatorially nor axially enter the small cavity of crown ether and hence is not well-encapsulated by the macromolecule. Therefore, the excimer prefers to stay on the exterior of the crown-ether, thus showing comparable lifetime of the excimer to that in aqueous medium. The internal radius of the cavity of α-CD is 5.7 Å[61] and can allow only axial encapsulation of the excimer but not equatorial. Consequently, the lifetime of the excimer in α-CD is more than that in crown ether but less than that in β-CD. The dimension of the dimer in the ground state (8 Å × 5 Å) is more than that of excimer, implying that possibility of encapsulation of the dimer by the organized media is less than that of excimer.

TRES and TRANES of 9AA between time 0 and 20 ns in CTAB medium are depicted in Figures 3 and 4, respectively. The observation of an isoemissive point at 504 nm in the TRANES profile indicates that the emission arises from two species, viz. monomer and excimer of 9AA. Similar TRES and TRANES profiles have also been obtained for aqueous and other heterogeneous media.

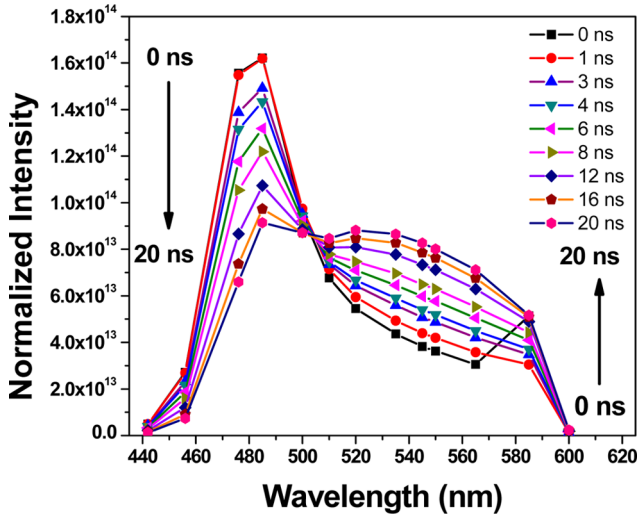

Figure 4. TRANES of 9AA (2.5×10^{-2} M) in 0.1 M CTAB between time 0 and 20 ns.

3.3. Steady-State Anisotropy Study. The study of steady-state fluorescence anisotropy of 9AA reveals the motional restriction imposed upon 9AA by the environment. Any factor that affects the size, shape, or segmental flexibility of a molecule will in turn affect the fluorescence anisotropy.[44]The increase in fluorescence anisotropy is a result of the increase in rigidity of the neighboring environment of the fluorophore. Figure 5 depicts a plot of variation of fluorescence anisotropy of

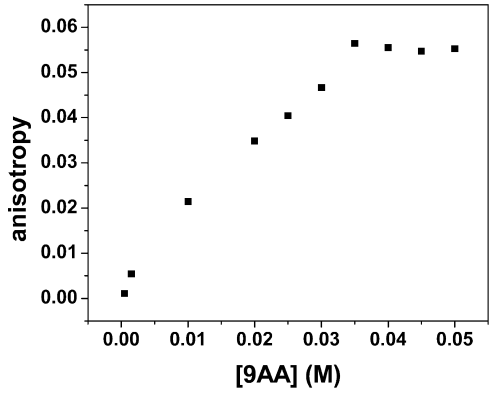

Figure 5. Variation of steady-state fluorescence anisotropy (r) of 9AA with increasing concentration in 0.1 M CTAB; [9AA] ranges from 5×10^{-4} to 5×10^{-2} M; λ_{ex} = 400 nm, λ_{em} = 535 nm.

9AA as a function of its concentration. The Figure shows a marked increase in the anisotropy (r) of 9AA on increasing concentration, implying that the motional freedom of the organic dye is restricted at higher concentration, which may be due to excimer formation.

3.4. Time-Resolved Fluorescence Anisotropy Studies. According to the Stokes–Einstein relationship[63]

dx.doi.org/10.1021/jp3103639 | J. Phys. Chem. A 2013, 117, 1428–1438

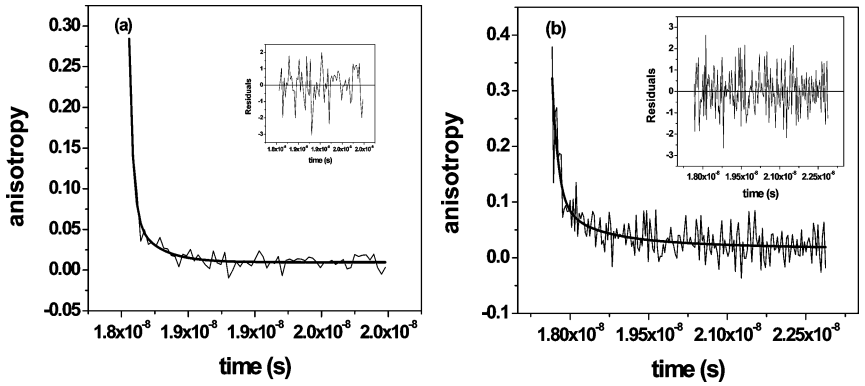

Figure 6. Time-resolved anisotropy decay curves for 9AA (a) monomer (5×10^{-5} M 9AA) and (b) excimer (2.5×10^{-2} M 9AA) in 0.1 M CTAB medium. λ_{ex} = 535 nm.

$$\tau_r = \frac{1}{6D_r}, \quad \text{where } D_r = \frac{RT}{6V\eta} \tag{6}$$

Here τ_r is the rotational correlation time, V is the hydrodynamic molecular volume, T is the absolute temperature, D_r is the rotational diffusion coefficient, and η is the viscosity of the medium. On the formation of excimer, the hydrodynamic molecular volume is expected to increase, which in turn may increase the rotational correlation time. Considering this fact, time-resolved anisotropy measurements are carried out at two different concentrations of the acridine dye solution. For the dilute solution of 9AA, where only monomer is expected to exist, the anisotropy decay fits to a single exponential function. The value of τ_r is too short to be detected with our TCSPC setup and is evaluated to be 0.11 ns. However, for a concentrated solution of 9AA, the anisotropy appears to be biexponential with two correlation times, a shorter component of 0.15 ns (23.15%.) and a longer component of 2.02 ns (76.85%). The existence of two components indicates the presence of two species, viz. monomer and excimer. The motional restriction imposed by the excimer formation is responsible for the emergence of the longer component of the rotational correlation time. Time-resolved anisotropy decay curves for 9AA are depicted in Figure 6.

3.5. Laser Flash Photolysis Study. To confirm the existence of the two forms of 9AA in the excited state, a laser flash photolysis study has been employed. The transient absorption spectra of 9AA in 10% CTAB at a time lag of 0.6 μs after laser flash at 355 nm are depicted in Figure 7. Each spectrum in Figure 7 shows prominent peaks at 340, 500, and 540 nm along with considerable bleaching around 400 nm, which is found to recover quickly, followed by an absorption growth. The presence of two isosbestic points at 370 and 435 nm possibly represents the existence of equilibrium between the monomer and excimer of 9AA. Another observation that is noteworthy is that the absorbance at 340, 500, and 540 nm of 9AA is almost the same at low concentration, where monomer species of 9AA predominates; however, the enhancement in absorbance at 500 and 540 nm with increase in concentration is more prominent compared with that at 340 nm. This indicates that probably the broad positive absorption in the region of 500−550 nm can be assigned to the excimer species of 9AA in the excited state.

Owing to the strong ground-state absorption of 9AA in the wavelength range of 380−420 nm, appreciable bleaching is observed in the transient absorption spectrum in the similar

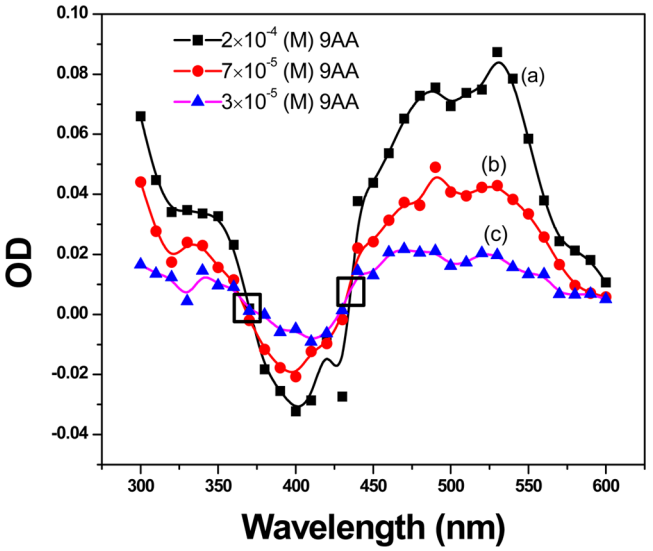

Figure 7. Transient absorption spectra of (a) 2×10^{-4} M 9AA (■), (b) 7×10^{-5} M 9AA (●), and (c) 3×10^{-5} M (▲) 9AA at 0.6 μs time delay after laser pulse with excitation wavelength at 355 nm in 10% CTAB.

range of wavelength, and this effect is more pronounced in the more concentrated solution. However, the bleaching is accompanied by a quick recovery, indicating the tendency of dimerization in the higher wavelength region. The recovery profiles at 400 nm are shown in Figure 8. The phenomena of bleaching and subsequent recovery represent the existence of a dynamic equilibrium between the monomer and excimer forms of 9AA, which is evident from the emergence of an isosbestic point at 435 nm.

The decay profiles of 9AA at 500 and 540 nm in 10% CTAB medium are shown in Figure 9. The confirmation of the fact that the monomer is the sole species existing at the low concentration range is that the lifetime obtained from the growth profile at 400 nm is almost the same as that obtained from the decay profile at 500 nm for low concentration of 9AA, as evident from Table 3. However, as the concentration of 9AA increases, the value of lifetime at a particular concentration obtained from the growth profile at 400 nm and the corresponding decay profile becomes unrelated, as shown in Table 3. This implies that at higher concentration some other species than the monomer exists in the solution, which in this

dx.doi.org/10.1021/jp3103639 | J. Phys. Chem. A 2013, 117, 1428−1438

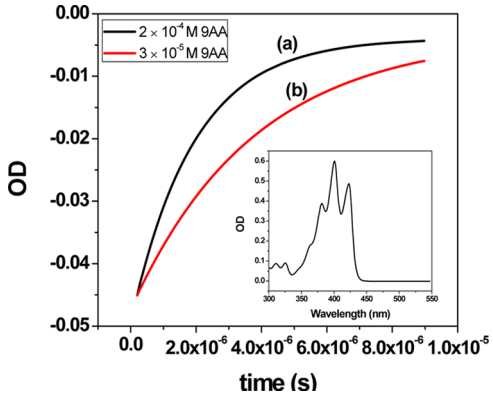

Figure 8. Normalized recovery profiles of (a) 2×10^{-4} M and (b) 3×10^{-5} M of 9AA in 10% CTAB medium at 400 nm (λ_{ex} = 355 nm). Inset shows the ground-state absorption of 9AA (6.5×10^{-5} M) in 10% CTAB medium.

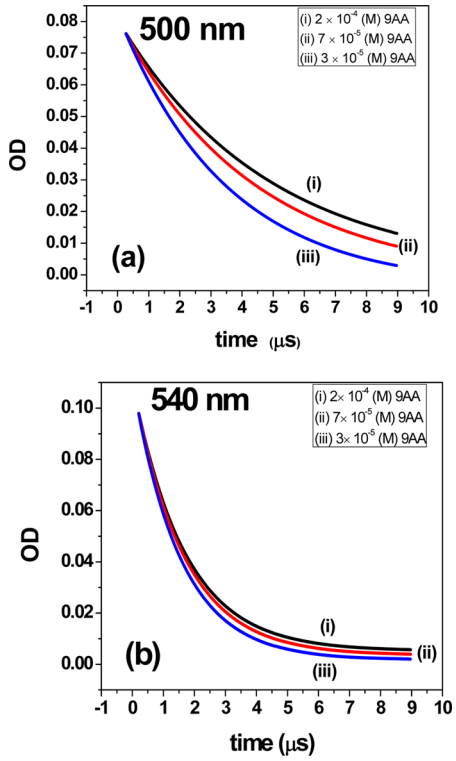

Figure 9. Normalized OD traces at (a) 500 and (b) 540 nm obtained by laser flash photolysis (λ_{ex} = 355 nm) of 9AA at various concentrations.

Table 3. Lifetime of 9AA with Variation in Concentration at 400 and 500 nm in 10% CTAB Medium

[9AA] (M)	τ at 400 nm (μs)	τ at 500 nm (μs)
3×10^{-5}	3.75	3.64
7×10^{-5}	3.09	4.34
2×10^{-4}	1.98	4.78

case is the excimer responsible for the differential values of lifetime obtained from the growth and decay curves.

3.6. Theoretical Study. A DFT-D, wB97XD, has been adopted instead of more popular DFT functionals, such as B3LYP, PB91, and so on, because it is well known that DFT methods do not consider the dispersion interaction, which is very important for $\pi-\pi$ stacking complexes.[64−68] We have used the DFT method for calculation of ground-state systems, whereas we have used TD-DFT for calculation of the excited state because several groups showed its usefulness in excimer property estimation.[25,69−76] The values of dipole moment of 9AA monomer in ground and excited states are very close to each other, as shown in Table 4, indicating the absence of electron transfer between two monomers forming dimers. The significantly large values of dipole moment of 9AA in both ground and excited states (~3.44 D) further rationalize why 9AA is not soluble in hydrophobic solvents, as indicated in Section 3.1. The energies of monomer as well as those of the dimers in ground and excited states are almost comparable, indicating that the potential energy barrier for transition from monomer to dimer or vice versa is very small in both the cases. Therefore, there is a possibility of existence of equilibrium between these two forms in both ground and excited states. Now, both the dimer and excimer after optimization with wB97XD/631G (2d, 2p) give stacked geometries. The values of interaction energies of ground-state dimer and excited-state dimer (excimer) are −17.44 and −23.06 kcal/mol, respectively, implying that the excimer is more stable by ~6 kcal/mol compared with the ground-state dimer. Moreover, from the optimized structures of both dimer and excimer, it can be easily understood that the stability of excimer is greater compared with dimer. The lesser overlap area of the ground-state complex possibly indicates that each monomer, even after stacking, has the capability to interact with another monomer, as depicted in Figure 10. It appears that the amino groups of 9AA can form hydrogen bonds (H bonds) with imino nitrogen atoms of another 9AA in both ground and excited states. Such hydrogen bond formation requires out-of-plane motion of the amino hydrogens, forming a pyramidal structure. Such pyramidalization was previously indicated to be the natural consequence of lone-pair electrons in the vicinity of aromatic system,[77] as in nucleic acid bases. Such pyramidalization was also shown to be important in cross-strand bifurcated hydrogen bonding between successive base-pairs of DNA, giving rise to enhanced rigidity to certain sequences.[78,79] In the ground state, there is a possibility of a single hydrogen bond between one of the hydrogen atoms of the amino groups, whereas in the excimer, both the hydrogen atoms of amino groups form a hydrogen bond with the imino nitrogen atoms. We have further observed a larger amount of pyramidalization of amino group nitrogen in the excimer, indicating lesser extended conjugation between lone-pair electrons of the nitrogen atoms with the pi-electron cloud. Details of the hydrogen bonding geometry are given in Tables 5 and 6. In the case of ground-state dimer, two of those four H-bond distances are comparatively larger, whereas in the case of excited-state dimer we find four hydrogen bonds of similar geometry (Table 5). From these theoretical data, one can presume that hydrogen-bond-like interaction can form between amino-H and imino-N atoms of 9AA in both ground- and excited-state dimer after optimization. As depicted in Table 6, two amino-N−amino-H bonds are naturally long compared with the other two, which confirms the possibility of two hydrogen bondings for ground-state dimer, but in the case of excimer all values are comparable. Thus in the excimer all four hydrogen atoms (amino-H atoms) of the two monomers are involved in H-bond formation with two imino-N atoms of the participating monomers. This is also supported by C9−amino-N bond distances, as depicted in Table 6. Owing to the formation of the H bonds as discussed above, the bond

dx.doi.org/10.1021/jp3103639 | J. Phys. Chem. A 2013, 117, 1428−1438

Table 4. Dipole Moments and Improper Dihedral Angles of 9AA of the Optimized Structures of Obtained through wB97XD/631G (2d, 2p)

systems	dipole moment (*D*)	improper dihedral angle (C9−N−H1−H2) (°)
monomer (ground state)	3.44	134.65
monomer (excited state)	3.48	137.55
dimer (ground state)	0.0064	127.52
		127.71
excimer	0.0259	134.85
		134.90

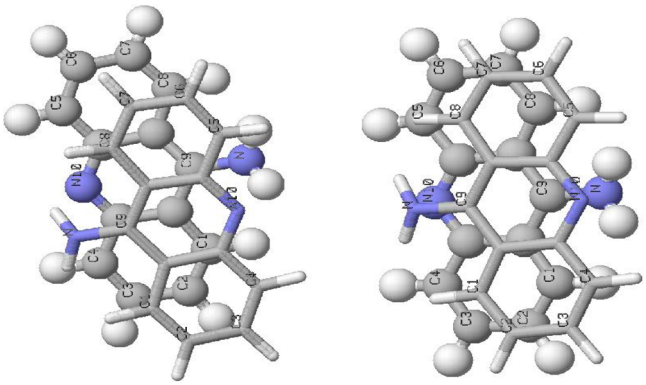

Figure 10. Optimized structures of dimer and excimer of 9AA.

Table 5. Hydrogen Bond Length (amino-Hs−Imino-N10) and Bond Angle of the Optimized Structures of Obtained through wB97XD/631G (2d, 2p)

systems	bond length (Å) (H−N)	bond angle (°) (N-H−N)
dimer	2.66	122.72
	2.65	122.62
excimer	2.71	96.39
	2.72	96.74
	2.71	96.48
	2.72	96.70

between amino-N and amino-H gets stretched, resulting in shortening of the C9−amino-N bond distance. In the case of excimer, this shortening of the C9−amino-N bond takes place to a greater extent compared with dimer (as depicted in Table 6), thus confirming that a greater number of hydrogen bonds is associated with the former than the latter. This would prohibit the excimer from the formation of additional interactions, thereby getting locked into dimers only.

As indicated in Tables 5 and 6, the hydrogen-bonding geometry is not indicative of strong attractions, leaving hydrogen bonding questionable. Thus, NBO analysis[80−82] of the systems in both forms is carried out. This approach includes all possible interactions between donor Lewis-type NBOs and acceptor non-Lewis NBOs. In this case, natural charges of the amino-H, imino-N, as well as amino-N, which are depicted in Table 7, are mainly taken into consideration. Charge modification takes place for both the amino-N and imino-N in the case of excimer and dimer with respect to the monomer species. Here imino-N behaves as an acceptor of H-bonding and amino-N behaves as donor. In the case of excimer, the donors (amino-N) become more positive and acceptors (imino-N) become more negative compared with 9AA monomer and dimer in the ground state, which indicates that the occurrence of H-bonding is much more for the excimer. Therefore, the extent of H-bonding is greater for excimer compared with dimer.

These results show that the probability of the formation of dimer of 9AA in the excited state is more than that in the ground state, which possibly accounts for the experimental finding that dimerization of 9AA is observed to occur only in the excited state.

4. CONCLUSIONS

We have made an attempt to explore the monomer and dimer equilibrium of 9AA in different media from both spectroscopic and theoretical point of views. The prime finding of this work is that 9AA dimerizes only in the excited state and not in the ground state. The absence of a new peak at higher concentration of 9AA in UV-spectroscopic study rules out the possibility of dimerization in the ground state. The occurrence of excimer formation is initially confirmed by the appearance of a new peak at higher concentration of 9AA in the steady-state fluorescence study. The presence of an isoemissive point in the TRANES profiles further implies the presence of two species of 9AA, viz. monomer and excimer. A more detailed picture of the monomer−excimer equilibrium is obtained from the flash photolysis study, which serves as supplementary evidence of the occurrence of the dimer in the excited state. The locking of two monomeric units of 9AA via four hydrogen bonds among the imino-N and amino-H in the excited state makes the excimer energetically more favorable compared with the dimer in the ground state, where the two

Table 6. Lengths (Å) of Various Covalent Bonds in Monomer (Excited and Ground States), Dimer, and Excimer of 9AA, Which Changed Due to Complexation or Excitation

systems	monomer (ground state)	monomer (excited state)	dimer (ground state)	excimer
amino-N−H	1.00634	1.00871	1.01138	1.00956
	1.00634	1.00869	1.00811	1.00959
			1.00811	1.00952
			1.01138	1.00957
C9−amino-N	1.37699	1.36829	1.37492	1.35920
C9−amino-N			1.37495	1.35908

dx.doi.org/10.1021/jp3103639 | J. Phys. Chem. A 2013, 117, 1428−1438

Table 7. Results from Natural Bond Orbital Analysis Characterizing Hydrogen Bond Formation between Imino-N and Amino-N−Amino-H Moiety of 9AA

system	monomer (ground state)	monomer (excited state)	dimer (ground state)	excimer
imino-N	−0.47432 e	−0.48720 e	−0.50566 e	−0.51241 e
			−0.50574 e	−0.51240 e
amino-N	−0.84299 e	−0.83866 e	−0.84090 e	−0.81921 e
			−0.84090 e	−0.81913 e
amino-H	0.41824 e	0.42395 e	0.42992 e	0.42995 e
	0.41825 e	0.42393 e	0.41767 e	0.42973 e
			0.41765 e	0.42992 e
			0.42988 e	0.42974 e

monomeric units are held together by only two such hydrogen bonds. Therefore, theoretical calculation proposes the preferential dimerization of 9AA in the excited state, thus substantiating the experimental findings. The extent of aggregation of the photosensitizer dye inside the cell membrane has a significant effect on the efficiency of PDT.[40] Hence, this detailed study of the formation of excimer in the confined environment mimicking biological cell membranes may add a new dimension to the prospect of 9AA as a drug in PDT.

AUTHOR INFORMATION

Corresponding Author

*Fax: (+91) 33-2337-4637. E-mail: samita.basu@saha.ac.in.

Author Contributions

‖Both authors contribute equally to this paper.

Notes

The authors declare no competing financial interest.

ACKNOWLEDGMENTS

Financial assistance from the Chemical and Biophysical Approaches for Understanding Natural Processes (CBAUNP) and Biomolecular Assembly, Recognition and Dynamics (BARD) projects, SINP of Department of Atomic Energy (DAE), Government of India is greatly acknowledged. P.M. acknowledges the Junior Research Fellowship from Council of Scientific and Industrial Research (CSIR), India. We would like to acknowledge Mr. Ajay Das SINP, Kolkata for his assistance in fluorescence lifetime measurements. We sincerely thank Mrs. Chitra Raha for her kind assistance and technical support.

REFERENCES

(1) Dakiky, M.; Němcova, I. Aggregation of *o,o′*-Dihydroxyazo Dyes-1. Concentration, Temperature, and Solvent Effect. *Dyes Pigm.* **1999**, *40*, 141−150.

(2) Nath, S.; Ghosh, S. K.; Panigrahi, S.; Pal, T. Photo-Induced Decolorization of Dimethylmethylene Blue with Selenious Acid: A Novel Method to Examine Selective Monomer-Dimer Distribution of the Dye in Micelle. *Spectrochim. Acta, Part A* **2005**, *61*, 2145−2151.

(3) Kemnitz, K.; Sakaguchi, T. Water-Soluble Porphyrin Monomer-Dimer Systems: Fluorescence Dynamics and Thermodynamic Properties. *Chem. Phys. Lett.* **1992**, *196*, 497−503.

(4) Asakura, T.; Ishida, M. A Nuclear Magnetic Resonance Study on Aggregation of an Azo Dye, Orange II, in Aqueous Solution. *J. Colloid Interface Sci.* **1989**, *130*, 184−189.

(5) Sagdinc, S.; Pir, H. Spectroscopic and DFT Studies of Flurbiprofen as Dimer and its Cu(II) and Hg (II) Complexes. *Spectrochim. Acta, Part A* **2009**, *73*, 181−194.

(6) Suzuki, S.; Morita, Y.; Fukui, K.; Stao, K.; Shiomi, D.; Takui, T.; Nakasuji, K. Aromaticity on the Pancake-Bonded Dimer of Neutral Phenalenyl Radical as Studied by MS and NMR Spectroscopies and NICS Analysis. *J. Am. Chem. Soc.* **2006**, *128*, 2530−2531.

(7) Brandán, S. A.; Lopez, F. M.; Montejo, M.; González, J. J. L.; Altabef, A. B. Theoretical and Experimental Vibrational Spectrum Study of 4-Hydroxybenzoic Acids as Monomer and Dimer. *Spectrochim. Acta, Part A* **2010**, *75*, 1422−1434.

(8) Aguiar, E. C.; Silva, J. B. P.; da.; Ramos, M. N. Theoretical Calculations of the Molecular Properties of Maleimide and its Dimer. *Spectrochim. Acta, Part A* **2008**, *71*, 5−9.

(9) Warshel, A.; Huler, E. Theoretical Evaluation of Potential Surfaces, Equilibrium Geometries and Vibronic Transition Intensities of Excimers: The Pyrene Crystal Excimer. *Chem. Phys.* **1974**, *6*, 463−468.

(10) Szalewicz, K.; Cole, S. J.; Kolos, W.; Bartlett, R. J. A Theoretical Study of the Water Dimer Interaction. *J. Chem. Phys.* **1988**, *89*, 3662−3673.

(11) Masunov, A.; Dannenberg, J. J. Theoretical Study of Urea. I. Monomers and Dimers. *J. Phys. Chem. A* **1999**, *103*, 178−184.

(12) Vala, M. T.; Hillier, I. H.; Rice, S. A.; Jortner, J. Theoretical Studies of Transannular Interactions. I. Benzene Excimer Fluorescence and the Singlet States of the Paracyclophanes. *J. Chem. Phys.* **1966**, *44*, 23−35.

(13) Jones, G., II; Vullev, V. I. Ground- and Excited-State Aggregation Properties of a Pyrene Derivative in Aqueous Media. *J. Phys. Chem. A* **2001**, *105*, 6402−6406.

(14) Furube, A.; Murai, A.; Tamaki, Y.; Watanabe, S.; Katoh, R. Effect of Aggregation on the Excited-State Electronic Structure of Perylene Studied by Transient Absorption Spectroscopy. *J. Phys. Chem. A* **2006**, *110*, 6465−6471.

(15) (a) Falcone, R. D.; Correa, N. M.; Biasutti, M. A.; Silber, J. J. Acid-Base and Aggregation Processes of Acridine Orange Base in n-Heptane/AOT/Water Reverse Micelles. *Langmuir* **2002**, *18*, 2039−2047. (b) McArthur, E. A.; Godbe, J. M.; Tice, D. B.; Weiss, E. A. A Study of the Binding of Cyanine Dyes to Colloidal Quantum Dots Using Spectral Signatures of Dye Aggregation. *J. Phys. Chem. C* **2012**, *116*, 6136−6142. (c) Mirenda, M.; Strassert, C. A.; Dicelio, L. E.; Román, E. S. Dye-Polyelectrolyte Layer-by-Layer Self-Assembled Materials: Molecular Aggregation, Structural Stability, and Singlet Oxygen Photogeneration. *ACS Appl. Mater. Interfaces* **2010**, *2*, 1556−1560. (d) Lu, H.-P.; Tsai, C.-Y.; Yen, W.-N.; Hsieh, C.-P.; Lee, C.-W.; Yeh, C.-Y.; Diau, E. W-G. Control of Dye Aggregation and Electron Injection for Highly Efficient Porphyrin Sensitizers Adsorbed on Semiconductor Films with Varying Ratios of Coadsorbate. *J. Phys. Chem. C* **2009**, *113*, 20990−20997. (e) Kim, S.; Ohulchanskyy, T. Y.; Pudavar, H. E.; Pandey, R. K.; Prasad, P. N. Organically Modified Silica Nanoparticles Co-encapsulating Photosensitizing Drug and Aggregation-Enhanced Two-Photon Absorbing Fluorescent Dye Aggregates for Two-Photon Photodynamic Therapy. *J. Am. Chem. Soc.* **2007**, *129*, 2669−2675. (f) Zhang, G.; Zhai, X.; Liu, M. Spacer-Controlled Aggregation and Surface Morphology of a Selenacarbocyanine Dye on Gemini Monolayers. *J. Phys. Chem. B* **2006**, *110*, 10455−10460. (g) Bujdák, J.; Iyi, N. Molecular Aggregation of Rhodamine Dyes in Dispersions of Layered Silicates: Influence of Dye Molecular Structure and Silicate Properties. *J. Phys. Chem. B* **2006**, *110*, 2180−2186.

(16) Bujdák, J. Effect of the Layer Charge of Clay Minerals on Optical Properties of Organic Dyes. A Review. *Appl. Clay Sci.* **2006**, *34*, 58−73.
(17) Chakraborty, B.; Basu, S. Interaction of Proflavin with Aromatic Amines in Homogeneous and Micellar Media: Photoinduced Electron Transfer Probed by Magnetic Field Effect. *Chem. Phys. Lett.* **2010**, *487*, 51−57.
(18) Chakraborty, B.; Singha Roy, A.; Dasgupta, S.; Basu, S. Magnetic Field Effect Corroborated with Docking Study to Explore Photoinduced Electron Transfer in Drug-Protein Interaction. *J. Phys. Chem. A* **2010**, *114*, 13313−13325.
(19) Chakraborty, B.; Basu, S. Deciphering the Host-Guest Chemistry of Acridine Yellow and Cucurbit[7]uril: An Integrated Spectroscopic and Calorimetric Study. *Chem. Phys. Lett.* **2011**, *507*, 74−79.
(20) Chakraborty, B.; Basu, S. Magnetic Field Effect on Electron Transfer Reactions of Acridine Yellow with Amines of Varied Structures in Homogeneous Medium. *Chem. Phys. Lett.* **2010**, *493*, 76−82.
(21) Chakraborty, B.; Basu, S. Study of Interaction of Proflavin with Triethylamine in Homogeneous and Micellar Media: Photoinduced Electron Transfer Probed by Magnetic Field Effect. *Chem. Phys. Lett.* **2009**, *477*, 382−387.
(22) Chakraborty, B.; Basu, S. Interaction of BSA with Proflavin: A Spectroscopic Approach. *J. Lumin.* **2009**, *129*, 34−39.
(23) Chakraborty, B.; Basu, S. Magnetic Field Effect on Photoinduced Electron Transfer Reaction Associated with Hydrogen Bond Formation in Homogeneous Medium. *Appl. Magn. Reson.* **2012**, *42*, 5−15.
(24) Sarangi, M. K.; Dey, D.; Basu, S. Influence of Heterogeneity of Confined Water on Photophysical Behavior of Acridine with Amines: A Time-Resolved Fluorescence and Laser Flash Photolysis Study. *J. Phys. Chem. A* **2011**, *115*, 128−135.
(25) Sarangi, M. K.; Bhattacharyya, D.; Basu, S. Influence of 2′-Deoxy Sugar Moiety on Excited-State Protonation Equilibrium of Adenine and Adenosine with Acridine Inside SDS Micelles: A Time-Resolved Study with Quantum Chemical Calculations. *Chem. Phys. Chem.* **2012**, *13*, 1−11.
(26) Sarangi, M. K.; Basu, S. Photophysical Behavior of Acridine with Amines within the Micellar Microenvironment of SDS: A Time-Resolved Fluorescence and Laser Flash Photolysis Study. *Phys. Chem. Chem. Phys.* **2011**, *13*, 16821−16830.
(27) Sarangi, M. K.; Basu, S. Associated Electron and Proton Transfer between Acridine and Triethylamine in AOT Reverse Micelles Probed by Laser Flash Photolysis with Magnetic Field. *Chem. Phys. Lett.* **2011**, *506*, 205−210.
(28) Topal, M. D. Molecular Mechanisms of Chemical Mutagenesis: 9-Aminoacridine Inhibits DNA Replication in Vitro by Destabilizing the DNA Growing Point and Interacting with the DNA Polymerase. *Biochemistry* **1984**, *23*, 2367−2372.
(29) Jordan, D. O.; Sansom, L. N. Interaction of Proflavine and 9-Aminoacridine with DNA at Temperatures below and above the Melting Temperature. *Biopolymers* **1971**, *10*, 399−410.
(30) Rehn, C.; Pindur, U. Molecular Modeling of Intercalation Complexes of Antitumor Active 9-Aminoacridine and a [*d*,*e*]-Anellated Isoquinoline Derivative with Base Paired Deoxytetranucleotides. *Monatsh. Chem.* **1996**, *127*, 645−658.
(31) Loechler, E. L.; King, J. Identification of the 9-Aminoacridine/DNA Complex Responsible for Photodynamic Inactivation of P22. *Biochemistry* **1986**, *25*, 5858−5864.
(32) Grzesiek, S.; Otto, H.; Dencher, N. A. ΔpH-Induced Fluorescence Quenching of 9-Aminoacridine in Lipid Vesicles is Due to Excimer Formation at the Membrane. *Biophys. J.* **1989**, *55*, 1101−1109.
(33) Steinhardt, J.; Krijn, J.; Leidy, J. G. Differences between Bovine and Human Serum Albumins: Binding Isotherms, Optical Rotatory Dispersion, Viscosity, Hydrogen Ion Titration, and Fluorescence Effects. *Biochemistry* **1971**, *10*, 4005−4015.
(34) Gangola, P.; Joshi, N. B.; Pant, D. D. Excimer Emission in 9-Aminoacridine Hydrochloride. *Chem. Phys. Lett.* **1981**, *80*, 418−421.
(35) Pant, D. D.; Joshi, G. C.; Tripathi, H. B. Photophysics of 9-Aminoacridinium Hydrochloride. *Pramana* **1986**, *27*, 161−170.
(36) Murza, A.; Alvarez-Méndez, S.; Sanchez-Cortes, S.; García-Ramos, J. V. Interaction of Antitumoral 9-Aminoacridine Drug with DNA and Dextran Sulfate Studied by Fluorescence and Surface-Enhanced Raman Spectroscopy. *Biopolymers* **2003**, *72*, 174−184.
(37) Murza, A.; Sánchez-Cortés, S.; García-Ramos, J. V.; Guisan, J. M.; Alfonso, C.; Rivas, G. Interaction of the Antitumor Drug 9-Aminoacridine with Guanidinobenzoatase Studied by Spectroscopic Methods: A Possible Tumor Marker Probe Based on the Fluorescence Exciplex Emission. *Biochemistry* **2000**, *39*, 10557−10565.
(38) Murza, A.; Sánchez-Cortés, S.; García-Ramos, J. V. Fluorescence and Surface-Enhanced Raman Study of 9-Aminoacridine in Relation to Its Aggregation and Excimer Emission in Aqueous Solution and on Silver Surface. *Biospectroscopy* **1998**, *4*, 327−339.
(39) Bae, S. I.; Zhao, R.; Snapka, R. M. PCNA Damage Caused by Antineoplastic Drugs. *Biochem. Pharmacol.* **2008**, *76*, 1653−1668.
(40) Delmarre, D.; Hioka, N.; Boch, R.; Sternberg, E.; Dolphin, D. Aggregation Studies of Benzoporphyrin Derivative. *Can. J. Chem.* **2001**, *79*, 1068−1074.
(41) Borisov, S. M.; Blinova, I. A.; Vasil'ev, V. V. The Influence of Dimerization of Water-Soluble Metalloporphyrins as Photosensitizers on the Efficiency of Generation of Singlet Oxygen. *High Energy Chem.* **2002**, *36*, 189−192.
(42) Tanielian, C.; Heinrich, G. Effect of Aggregation on the Hematoporphyrin-Sensitized Production of Singlet Molecular Oxygen. *Photochem. Photobiol.* **1995**, *61*, 131−135.
(43) Tanielian, C.; Schweitzer, C.; Mechin, R.; Wolff, C. Quantum Yield of Singlet Oxygen Production by Monomeric and Aggregated Forms of Hematoporphyrin Derivative. *Free Radical Biol. Med.* **2001**, *30*, 208−212.
(44) Lakowicz,J. R. *Principles of Fluorescence Spectroscopy*; Plenum Press: New York, 2006.
(45) Koti, A. S. R.; Periasamy, N. Application of Time Resolved Area Normalized Emission Spectroscopy to Multicomponent Systems. *J. Chem. Phys.* **2001**, *115*, 7094−7099.
(46) Koti, A. S. R.; Krishna, M. M. G.; Periasamy, N. Time-Resolved Area-Normalized Emission Spectroscopy (TRANES): A Novel Method for Confirming Emission from Two Excited States. *J. Phys. Chem. A* **2001**, *105*, 1767−1771.
(47) Maroncelli, M.; Fleming, G. R. Picosecond Solvation Dynamics of Coumarin 153: The Importance of Molecular Aspects of Solvation. *J. Chem. Phys.* **1987**, *86*, 6221−6239.
(48) Schaftenaar, G.; Noordik, J. H. Molden: A Pre- and Post-Processing Program for Molecular and Electronic Structures. *J. Comput.-Aided Mol. Des.* **2000**, *14*, 123−134.
(49) *Discovery Studio 2.5 Guide*; Accelrys, Inc.: San Diego, CA, 2009.
(50) Chai, J.-D.; Head-Gordon, M. Long-Range Corrected Hybrid Density Functionals with Damped Atom-Atom Dispersion Corrections. *Phys. Chem. Chem. Phys.* **2008**, *10*, 6615−6620.
(51) Frisch, M. J.; Trucks, G. W.; Schlegel, H. B.; Scuseria, G. E.; Robb, M. A.; Cheeseman, J. R.; Sclmani, G.; Barone, V.; Mennucci, B.; Petersson, G. A. et al. *Gaussian 09*, revision A.1; Gaussian, Inc.: Wallingford, CT, 2009.
(52) Bauernschmitt, R.; Ahlrichs, R. Treatment of Electronic Excitations within the Adiabatic Approximation of Time Dependent Density Functional Theory. *Chem. Phys. Lett.* **1996**, *256*, 454−464.
(53) Casida, M. E.; Jamorski, C.; Casida, K. C.; Salahub, D. R. Molecular Excitation Energies to High-Lying Bound State From Time-Dependent Density-Functional Response Theory: Characterization and Correction of the Time-Dependent Local Density Approximation Ionization Threshold. *J. Chem. Phys.* **1998**, *108*, 4439−4449.
(54) Stratmann, R. E.; Scuseria, G. E.; Frisch, M. J. An Efficient Implementation of Time-Dependent Density-Functional Theory for the Calculation of Excitation Energies of Large Molecules. *J. Chem. Phys.* **1998**, *109*, 8218−8224.

(55) Caillie, C. V.; Amos, R. D. Geometric Derivatives of Excitation Energies Using SCF and DFT. *Chem. Phys. Lett.* **1999**, *308*, 249−255.
(56) Caillie, C. V.; Amos, R. D. Geometric Derivatives of Density Functional Theory Excitation Energies Using Gradient-Corrected Functionals. *Chem. Phys. Lett.* **2000**, *317*, 159−164.
(57) Furche, F.; Ahlrichs, R. Adiabatic Time-Dependent Density Functional Methods for Excited State Properties. *J. Chem. Phys.* **2002**, *117*, 7433−7447.
(58) Scalmani, G.; Frisch, M. J.; Mennucci, B.; Tomasi, J.; Cammi, R.; Barone, V. Geometries and Properties of Excited States in the Gas Phase and in Solution: Theory and Application of a Time-Dependent Density Functional Theory Polarizable Continuum Model. *J. Chem. Phys.* **2006**, *124*, 094107 (1−15).
(59) Boys, S. F.; Bernardi, F. The Calculation of Small Molecular Interactions by the Differences of Separate Total Energies. Some Procedures with Reduced Errors. *Mol. Phys.* **1970**, *19*, 553−566.
(60) Sandeep, P.; Bisht, P. B. Photophysics of 9-Amino Acridine Hydrochloride Hydrate Single Microcrystal. *Chem. Phys.* **2006**, *326*, 521−526.
(61) Szejtli, J. Introduction and General Overview of Cyclodextrin Chemistry. *Chem. Rev.* **1998**, *98*, 1743−1753.
(62) Maleknia, S.; Brodbelt, J. Cavity-Size-Dependent Dissociation of Crown Ether/Ammonium Ion Complexes in the Gas Phase. *J. Am. Chem. Soc.* **1993**, *115*, 2837−2843.
(63) Valuer, B. *Molecular Fluorescence Principles and Applications*; VCH: Weinheim, Germany, 2002.
(64) Kristyán, S.; Pulay, P. Can (Semi) Local Density Functional Theory Account for the London Dispersion Forces? *Chem. Phys. Lett.* **1994**, *229*, 175−180.
(65) Pérez-Jordá, J. M.; Becke, A. D. A Density-Functional Study of van der Waals Forces: Rare Gas Diatomics. *Chem. Phys. Lett.* **1995**, *233*, 134−137.
(66) Hobza, P.; Sponer, J.; Reschel, T. Density Functional Theory and Molecular Clusters. *J. Comput. Chem.* **1995**, *16*, 1315−1325.
(67) Ortmann, F.; Schmidt, W. G.; Bechstedt, F. Attracted by Long-Range Electron Correlation: Adenine on Graphite. *Phys. Rev. Lett.* **2005**, *95*, 186101−186104.
(68) Ehrlich, S.; Moellmann, J.; Grimme, S. Dispersion-Corrected Density Functional Theory for Aromatic Interactions in Complex Systems. *Acc. Chem. Res., June 15*, **2012**.
(69) Jacquemin, D.; Wathelet, V.; Perpète, E. A.; Adamo, C. Extensive TD-DFT Benchmark: Singlet-Excited States of Organic Molecules. *J. Chem. Theory Comput.* **2009**, *5*, 2420−2435.
(70) Guillaumont, D.; Nakamura, S. Calculation of the Absorption Wavelength of Dyes using Time-Dependent Density-Functional Theory (TD-DFT). *Dyes Pigm.* **2000**, *46*, 85−92.
(71) Halls, M. D.; Schlegel, H. B. Molecular Orbital Study of the First Excited State of the OLED Material Tris(8-hydroxyquinoline)-aluminum(III). *Chem. Mater.* **2001**, *13*, 2632−2640.
(72) Gutavsson, T.; Bányász, A.; Lazzarotto, E.; Markovitsi, D.; Scalmani, G.; Frisch, M. J.; Barone, V.; Improta, R. Singlet Excited-State Behavior of Uracil and Thymine in Aqueous Solution: A Combined Experimental and Computational Study of 11 Uracil Derivatives. *J. Am. Chem. Soc.* **2006**, *128*, 607−619.
(73) Romaniello, P.; Lelj, F. Limits in the Second-Order Response of [M(H_2imXdt) (H_2imYdt)] Neutral Complexes (M = Ni, Pd, Pt; H_2imXdt = Monoanion of Imidazolidine-2-Chalcogenone-4,5-Dithione; X = O, S, Se; Y = O, S, Se; X ≠ Y): A Pure Theoretical Study Based on TD-DFT Approach and ZORA Formalism. *J. Mol. Struct.: THEOCHEM* **2003**, *636*, 23−37.
(74) Tretiak, S. Triplet State Absorption in Carbon Nanotubes: A TD-DFT Study. *Nano Lett.* **2007**, *7*, 2201−2206.
(75) Wu, C.; Tretiak, S.; Chernyak, V. Y. Excited States and Optical Response of a Donor-Acceptor Substituted Polyene: A TD-DFT Study. *Chem. Phys. Lett.* **2007**, *433*, 305−311.
(76) Shen, L.; Ji, H.-F.; Zhang, H.-Y. A TD-DFT Study on Triplet Excited-State Properties of Curcumin and Its Implications in Elucidating the Photosensitizing Mechanisms of the Pigment. *Chem. Phys. Lett.* **2005**, *409*, 300−303.
(77) Mukherjee, S.; Majumdar, S.; Bhattacharyya, D. Role of Hydrogen Bonds in Protein-DNA Recognition: Effect of Nonplanar Amino Groups. *J. Phys. Chem. B* **2005**, *109*, 10484−10492.
(78) Bandyopadhyay, D.; Bhattacharyya, D. Estimation of Strength in Different Extra Watson-Crick Hydrogen Bonds in DNA Double Helices through Quantum Chemical Studies. *Biopolymers* **2006**, *83*, 313−325.
(79) Bhattacharyya, D.; Kundu, S.; Thakur, A. R.; Majumdar, R. Sequence Directed Flexibility of DNA and the Role of Cross-strand Hydrogen Bonds. *J. Biomol. Struct. Dyn.* **1999**, *17*, 289−300.
(80) Carpenter, J. E.; Weinhold, F. Analysis of the Geometry of the Hydroxymethyl Radical by the "Different Hybrids for Different Spins" Natural Bond Orbital Procedure. *J. Mol. Struct.: THEOCHEM* **1988**, *169*, 41−62.
(81) Reed, A. E.; Weinstock, R. B.; Weinhold, F. Natural Population Analysis. *J. Chem. Phys.* **1985**, *83*, 735−746.
(82) Reed, A. E.; Curtsiss, L. A.; Weinhold, F. Intermolecular Interactions from a Natural Bond Orbital, Donor-Acceptor Viewpoint. *Chem. Rev.* **1988**, *88*, 899−926.